LAWRENCE
LIVERMORE
NATIONAL
LABORATORY

LLNL-PROC-825973

Lens-coupled MeV X-Radiography with Transparent Ceramic GLO Scintillators

N. J. Cherepy

August 23, 2021

SPIE - Hard X-Ray, Gamma-Ray, and Neutron Detector Physics XXIII
San Diego, CA, United States
August 1, 2021 through August 5, 2021

Disclaimer

Lens-coupled MeV X-Radiography and CT with Transparent Ceramic GLO Scintillators

N.J. Cherepy, Z.M. Seeley, D.J. Schneberk, C.J. McNamee, C.I. Pincus, T.J. Rudzik, R.A. Osborne, I.R. Phillips, J.A. Nicolino, J. Hall, A. Townsend, S.A. Payne

Lawrence Livermore National Laboratory, Livermore, CA 94550, USA

ABSTRACT

High energy X-ray CT can provide 3-D volumetric views of complex multi-material objects. We have developed a new polycrystalline transparent ceramic scintillator, $Gd_{0.3}Lu_{1.6}Eu_{0.1}O_3$, or "GLO," that offers excellent X-ray stopping power at MeV energies (α_γ = 0.36 cm^{-1} at 3 MeV), high scintillation light yield (55,000 Ph/MeV) in sizes up to 14" x 14" plates and thicknesses of 2-4 mm, with high intrinsic spatial resolution. GLO can provide improved contrast and increased imaging throughput for MeV Bremsstrahlung X-ray computed tomography, compared to standard glass and phosphor scintillator screens. Imaging studies conducted with a 7.8 MeV endpoint energy Bremsstrahlung X-ray source using a lens-coupled GLO plate imaged on a sCMOS camera high spatial resolution of <100 µm, as measured with a wire-pair gauge. X-ray computed tomography with GLO could measure tungsten wires as small as 63 µm behind 6 mm of copper, <1 mm^3 voids in plastic behind several millimeters of aluminum and tungsten, and intentionally included voids in the few-hundred-microns range in the interior of a 9 cm diameter additively manufactured Inconel phantom.

Keywords: X-ray radiography, MeV X-ray, X-ray computed tomography, Ceramic Scintillators, Transparent Ceramics

1. INTRODUCTION

Lens-coupled X-ray computed tomography (X-ray CT) using a transparent scintillator imaged on a CCD or sCMOS camera obtains higher spatial resolution than the more commonly employed phosphor-enhanced amorphous silicon (A-Si) panels [1]. A-Si panels are limited to resolution on the order of 100-200 microns, have a limited working life due to degradation with dose, and provide intrinsically low efficiency with thin (few hundred µm thick) phosphor coatings, such as "DRZ-enhanced" Gadolinium Oxysulfide or Cesium Iodide (Figure 1). The A-Si panels encounter "fill factor" effects and require thin scintillators to generate an image with sufficient intrinsic resolution. Thin scintillators have poor stopping power, and the result is less contrast, more beam filtration and longer scan times – reducing the per-scan lifetime of the detector. As an alternative, thicker ~3 mm GLO plates may be lens-coupled for higher efficiency and resolution, at the cost of added complexity of requiring a mirror, lens and a shielded low-noise camera for readout.

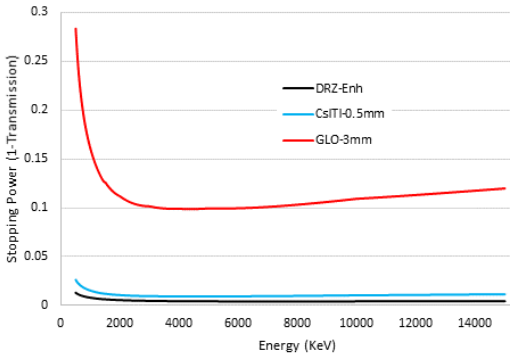

Figure 1. Comparison of stopping power for different scintillators used in X-ray CT. Amorphous silicon panels are typically enhanced with Gadox or Gd_2O_2S:Tb phosphor coatings, such as DRZ-Enh (200 µm screen) or CsI:Tl columnar structures. Lens-coupled GLO can be thicker, in the 2-4 mm range, while retaining ~100 µm resolution.

For large fields-of-view, very large area but thin transparent scintillators are required – a format difficult to fabricate with high-light-yield single crystals. As a result, glass scintillators with both modest X-ray interaction and light yield are typically used [3]. The higher stopping power and light yield of GLO enables the CT imaging of the interior of complex additively manufactured high-attenuating components (Inconel, Niobium) at high effective scan energy (see Figure 1), with high contrast and high spatial resolution [2], as may be achieved with a lens-coupled system (Figure 2). The result is high performance CT imaging at higher energies with shorter scan times at small pixel sizes than is obtained with A-Si panels or with alternative scintillators in a lens-coupled configuration.

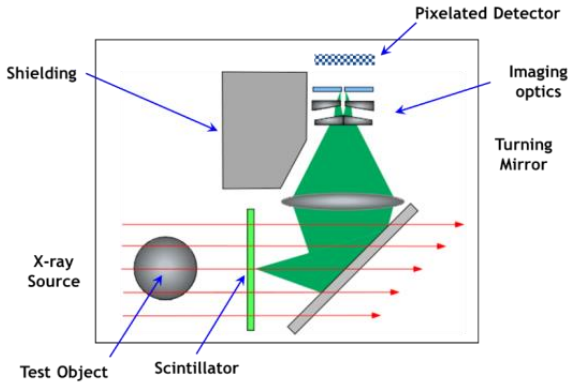

Figure 2. Typical lens-coupled imaging configuration.

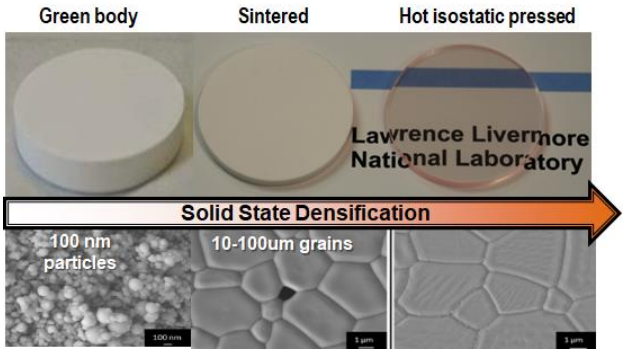

Figure 3. Transparent ceramics fabrication process.

Phase-pure, transparent, polycrystalline $Gd_{0.3}Lu_{1.6}Eu_{0.1}O_3$, or "GLO" ceramics are a variant of the simpler compound, Lu_2O_3 [4], but offering improved transparency when formed as ceramics. Fabrication of transparent ceramics uses nanoparticle feedstock that is hot-pressed, vacuum-sintered, and then hot-isostatic-pressed to full density [5,6]. Figure 3 shows the key fabrication steps, from left-to-right, as the nanoparticles are pressed into a green body, the grain size increases upon sintering to 10-100 microns, and finally all the voids are pressed out with a hot isostatic pressing step. GLO is reproducibly formed with acceptably low optical scatter losses (<10%/cm) for use in lens-coupled imaging [7]. In addition to its high light yield of 55,000 Photons/MeV, GLO offers excellent X-ray stopping, due to its Z_{eff} = 68 and density of 9.1 g/cm^3.

2. EQUIPMENT AND METHODS

2.1 Imaging configuration

GLO scintillator plates were fabricated following established procedures [5,6]. X-ray attenuation radiographs were acquired using a 7.8 MeV Bremsstrahlung source with 1.8 mm spot size at the Radiabeam with the ARCIS LINAC (Santa Monica, CA). The imaging system was configured with lead collimators, Newport RV160CC rotary table, a 2.6 mm thick GLO scintillator, turning mirror, Nikon Nikkor lens and ZYLA 5.5 sCMOS camera (42 µm pixel pitch at focus). Radiographs were flat-field corrected, background subtracted and processed for computed tomography performed with JILREC software [7].

2.2 Imaging Phantoms

Several imaging phantoms were developed to explore the resolution and contrast that could be obtained with 7.8 MeV Bremsstrahlung imaging. A duplex wire penetrameter was used to determine the smallest wire readily detectable. Phantom 1 (Figure 4) features a wire gauge set shielded between a copper shell and an interior aluminum cylinder.

Phantom 2 (Figure 5) consists of an outer aluminum shell, inner tungsten shell and four different high-density polyethylene (HDPE) inserts, each with various precision machined voids. Phantom 3 is a 9 cm diameter Inconel cylinder with 5 sets of embedded holes: 380 µm, 889 µm, 1.65 mm, 3.43 mm, 5.21 mm.

Figure 4. Phantom 1 includes an outer copper shell (6.35 mm thick) and inner aluminum cylinder (38.1 mm diameter), each with various voids. A wire gauge penetrameter was inserted in the interstitial space between the Cu and Al.

Figure 5. Another multi-material phantom is comprised of an outer aluminum shell, inner tungsten shell and a series of high-density polyethylene (HDPE) central inserts. Each HDPE insert has different voids, ranging from 0.5-3 mm diameter (top row shows CAD renderings of the inserts for visual clarity).

3. RESULTS AND DISCUSSION

3.1 Transparent ceramic GLO ($Gd_{0.3}Lu_{1.6}Eu_{0.1}O_3$) plates

Over the past five years, LLNL has worked with multiple vendors on the multi-stage processing and fabrication of large-size transparent ceramics. The route that we have found most reproducible uses flame spray pyrolysis-synthesized nanopowder from Nanocerox (Ann Arbor, MI), which is hot pressed to 1275°C, then vacuum sintered to 1640°C, followed by hot isostatic pressing to 1900°C. The resulting plates are then ground flat and parallel in a Blanchard grinder and then polished with diamond paste to produce a mirror-like surface finish. Subsequently, the edges and back side are painted with black paint, so that the scintillation only emerges from the front face toward the mirror. Figure 6 shows four of the plates produced via these methods, qualitatively displaying their transparency. Bulk transparency is excellent, with optical scatter at the scintillation wavelength of <10%/cm, but with occasional scatter centers with diameter of 0.2-2 mm, which limit exposure time due to their brightness, but in most cases may be removed during image processing by standard flat-fielding and background subtraction [8].

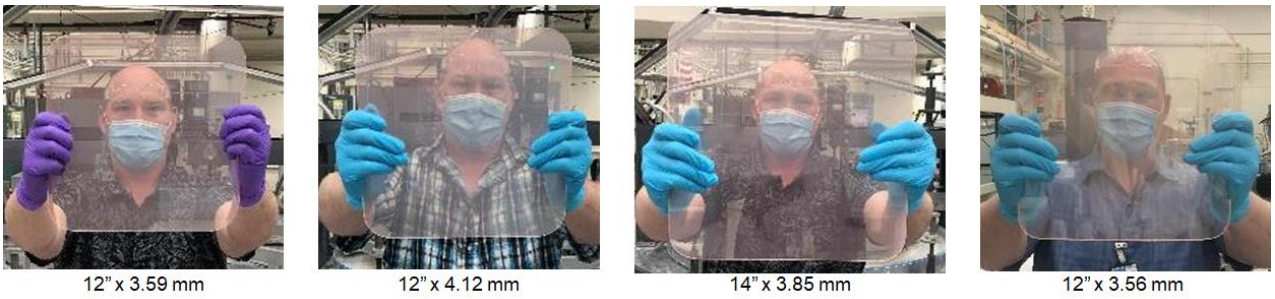

Figure 6. Multiple large-format GLO scintillator plates.

3.2 Radiography results

Like AMSI panels, radiographic images from camera-based systems are processed via additional metadata to obtain a more quantitative image of x-ray transmission and attenuation through an object or assembly. Acquired camera images (I_S), are processed with two other images (I_D and I_F) to accurately measure the detected x-ray interactions with the object, independent of the detector[9]. I_D is the Dark Image, a measure of the counts due to the thermal load on the camera sensor which is acquired with no beam and no object. I_F is the Flat Field Image or Irradiance Reference image, which is acquired with beam on, but no object. I_F allows for correction of fixed pattern detector noise (including discrete scatter centers in the scintillator). Two types of processed radiographs are regularly produced with these images, I_{Tr} and I_{Att}, defined in Equations 1 and 2 [9]. Attenuation images are the input data for CT processing and reconstruction.

Eq. 1 $$Transmission\ Radiograph = I_{Tr} = \frac{I_S - I_D}{I_F - I_D}$$

Eq. 2 $$Attenuation\ Radiograph = I_{Att} = -ln\left[\frac{I_S - I_D}{I_F - I_D}\right]$$

Figure 7 shows a transmission radiograph of a duplex wire gauge, placed in contact with the scintillator. The three largest wire pairs in the duplex wire gauge are tungsten and the remaining wires are platinum. All of the wires are detectable, and the corresponding feature sizes listed in Table 1 reveal a system-level resolution for radiography of <100 µm. While these experiments constitute a practical laboratory demonstration, spatial resolution may be improved in the future with a higher quality lens system, camera with smaller pixel size, source configured for smaller X-ray beam spot size, and the use of a longer distance from the source to the object.

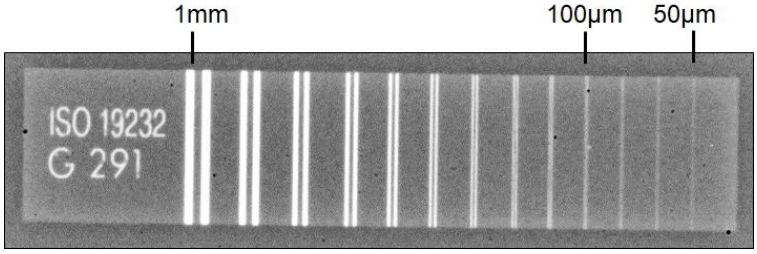

Figure 7. Transmission radiograph acquired with lens-coupled imaging, a 2.5 mm thick GLO plate, and the 7.8 MeV X-ray source. The effective spatial resolution of the system for transmission radiography is <100 µm.

Table 1. Duplex wire gauge provides quantitative resolution performance for the system.

Duplex wire number	Unsharpness (mm)	LP (1/mm)	Wire diameter and spacing (mm)
D3	1.000	1.000	0.500
D4	0.800	1.250	0.400
D6	0.500	2.000	0.250
D7	0.400	2.500	0.200
D8	0.320	3.130	0.160
D9	0.260	3.850	0.130
D10	0.200	5.000	0.100
D11	0.160	6.250	0.080
D12	0.130	7.690	0.063
D13	0.100	10.000	0.050

3.3 Computed tomography results

Phantom 1

A 360-degree scan of 600 equal-angular attenuation radiographs were acquired and reconstructed to characterize Phantom 1 (scan time < 1 hour). This phantom is comprised of an outer copper shell (6.35 mm thick), inner aluminum cylinder (38.1 mm diameter), and holds a tungsten wire gauge (W 13 FE, with smallest individual wire 50 µm). The CT reconstruction and image analysis readily detects <100 µm wires (Figure 5). The detection of these tiny wires behind the copper and aluminum shielding attests to the contrast and resolution capability of a lens-coupled GLO system for X-ray computed tomography of complex objects.

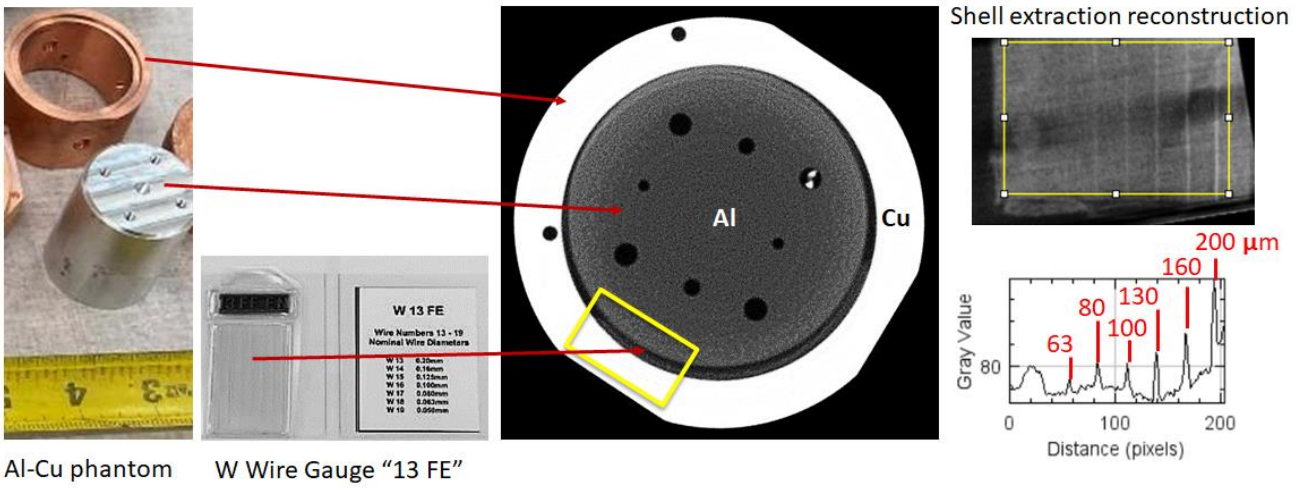

Figure 8. **(left)** Photos of the constituent parts of Phantom 1 – an outer copper shell and inner aluminum cylinder, with a W 13 FE wire gauge penetrameter in the interstitial space between the copper and aluminum. **(middle)** CT reconstruction of the object, **(right)** Shell extraction slice shows the wires, and when the shell extraction slice is binned, the "swath out" shown at the bottom reveals wires smaller than 100 µm diameter.

Phantom 2

Phantom 2 is comprised of an outer 2 mm thick Al shell, inner 4 mm thick W shell and four different 10 mm diameter replaceable plastic (HDPE) inserts (see photos in Figure 4). Four configurations correlate with each of the different HDPE inserts. For each configuration, 600 views over 360 degrees were acquired, processed as described in Equation 2, and reconstructed using JILREC. Figures 9-12 quantify the system performance for detection of small voids in plastics behind shielding. For Figures 9-11, the shell extraction of the annulus that most clearly shows the HDPE features is shown at the top, with a binned "swath out" and CAD drawings. At the bottom, slices progressing through the volume of the phantom are shown, and the slice that most clearly reveals the structure in the HDPE insert is boxed in red.

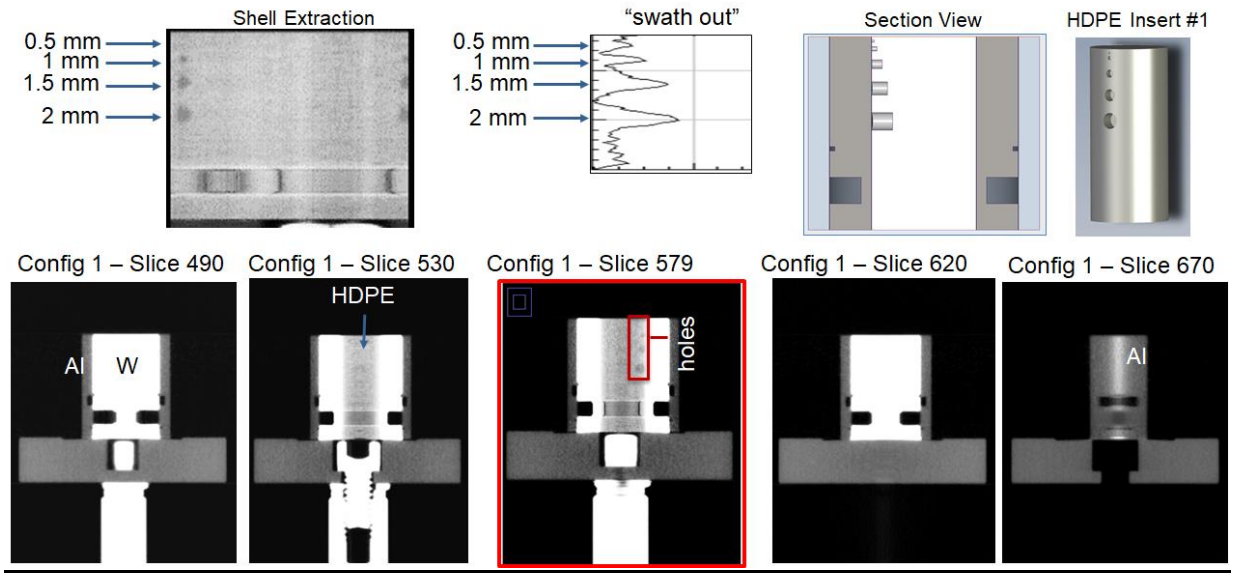

Figure 9. Phantom 2, assembled in Configuration 1 has small cylindrical voids in the plastic (HDPE) insert. Voids are found to be detectable behind Al and W shielding down to 1 mm diameter x 1 mm tall (0.79 mm^3). The contrast for the smallest feature, 0.5 mm x 0.5 mm (0.1 mm^3) is comparable to the noise.

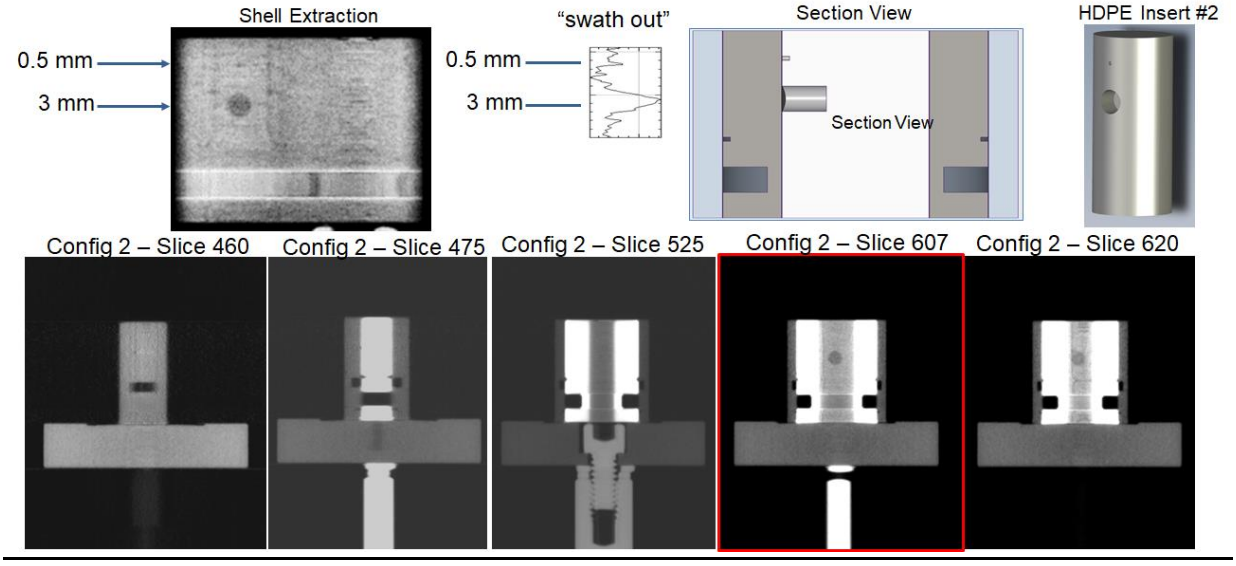

Figure 10. Phantom 2, Configuration 2 has small cylindrical voids in the plastic (HDPE) insert. While the 3 mm void (10.6 mm^3) is readily detectable behind Al and W shielding the 0.5 mm x 0.5 mm (0.1 mm^3) is comparable to the noise.

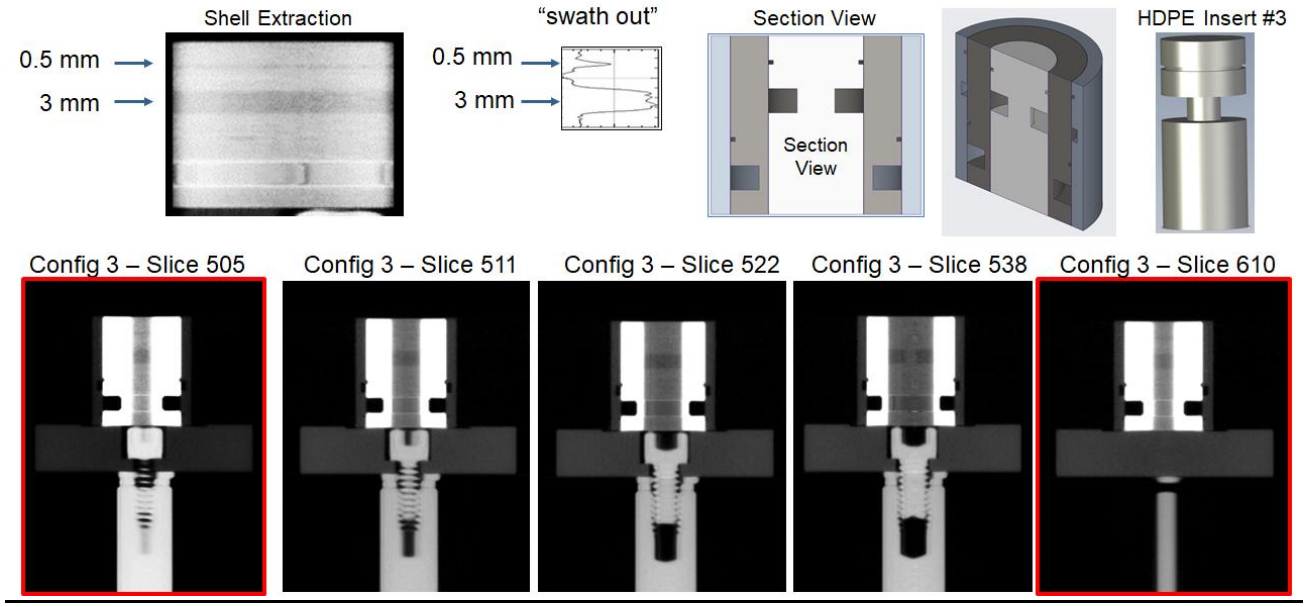

Figure 11. Phantom 2, Configuration 3 has grooves cut into the circumference of the plastic (HDPE) insert. Both the 3 mm (94.2 mm^3) and the 0.5 mm (15.7 mm^3) grooves are readily detectable behind Al and W shielding.

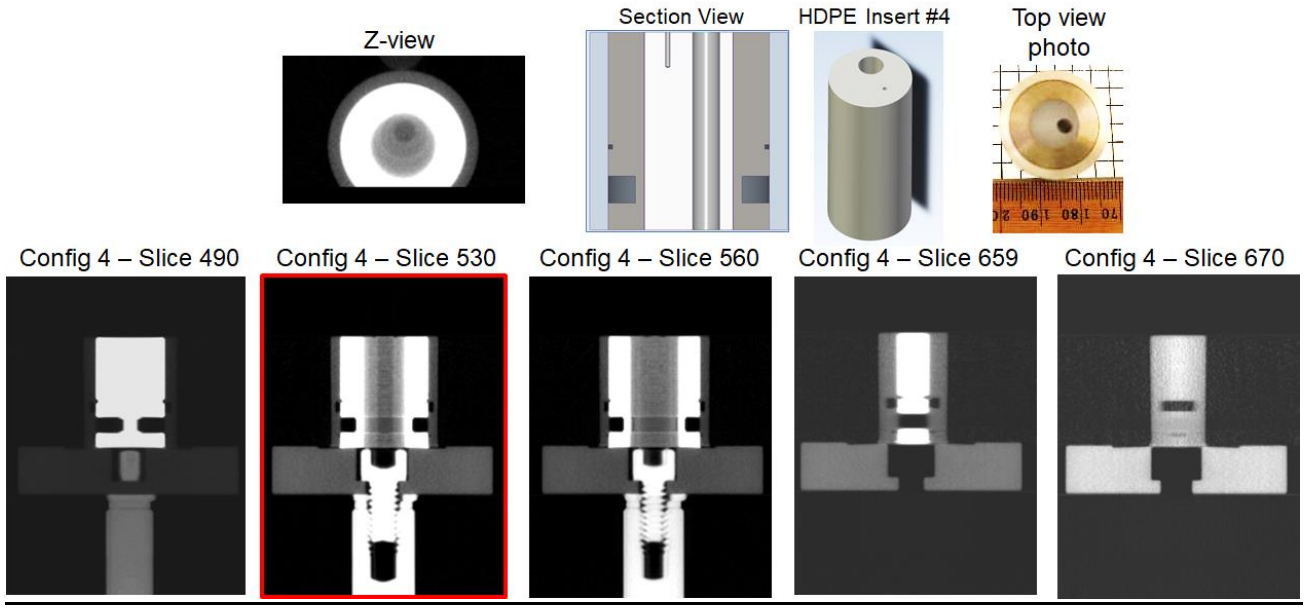

Figure 12. Phantom 2, Configuration 4 has a 3 mm vertical cylindrical through-hole (70 mm^3) and a shallow 0.25 mm cylindrical void (0.012 mm^3) drilled into the plastic (HDPE) insert. While the large 3 mm diameter hole is readily detectable behind Al and W shielding, the tiny 0.25 mm diameter void is not.

Phantom 3

The horizontal field of view for the current system at RADIABEAM (ARCIS LINAC Bay) is 10 cm. This resulted in a magnified projection just larger than the field of view. Consequently, we elected to acquire an offset-scan [9], where the object, rotational table and beam center are shifted to one side of the detector (with the rotational center always in the field of view for the scan) – and a 360-degree scan was acquired. To account for the reduction in data for the reconstructed voxels in an offset-scan we acquired 1200 views. The CT cross-sectional slice in Figure 13 shows that all of the embedded holes down to the smallest (0.015" or 380 µm) are resolved for this highly attenuating phantom.

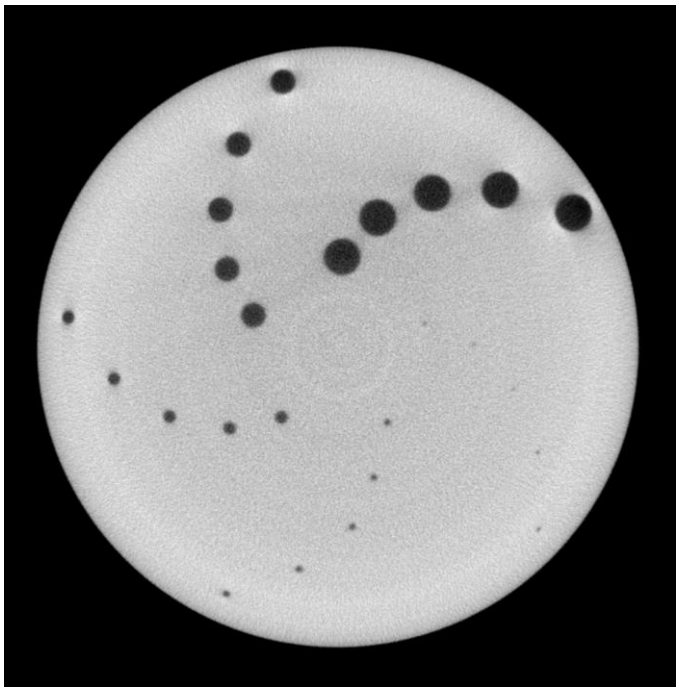

Figure 13. Cross-sectional slice of a 9-cm-diameter Inconel cylinder with embedded holes (380 µm, 889 µm, 1.65 mm, 3.43 mm, 5.21 mm), extracted from the X-ray CT acquired via lens-coupled imaging using a 2.5 mm thick GLO plate and 7.8 MeV X-ray source.

4 CONCLUSIONS

Transparent ceramic GLO scintillator plates can improve imaging performance for MeV radiography and CT. High energy, high-resolution CT volumetric scans can be acquired with short acquisition times for high attenuating additively manufactured objects and assemblies. Recently, GLO has been scaled up to 14" optically transparent plates that offer spatial resolution of <100 µm for transmission radiography with an off-the-shelf sCMOS camera and lens, using a 7.8 MeV Bremsstrahlung X-ray source. Computed tomography of complex objects was performed with this system and found to be able to detect fine Tungsten wires of diameters smaller than 100 µm diameter. CT was also capable of detecting precision machined voids in a shielded plastic phantom down to <1 mm^3 in various geometries, such as grooves and holes. While the contrast in the plastic components was poor, it did not impede the feature detection and identification down to about 100 µm diameter. Highly attenuating additively manufactured components require methods for evaluating internal defects, and X-ray CT with GLO is shown to accurately locate hundred-microns-scale porosity inside a 9 cm diameter Inconel cylinder. Improved contrast might be obtained with a lower energy source, but traversing dense material will become problematic at lower energies. While these results are promising, future work to improve performance will likely involve lower noise cameras, a lens system with reduced optical aberration, improved collimation of the beam, reduction in beam spot size, and optimization of source-to-object distance.

ACKNOWLEDGEMENTS

Thanks to the many collaborators on these efforts, including staff at Pantex, Los Alamos, Y-12, Varian, VJ Technologies, Radiabeam, CoorsTek, TA&T, American Isostatic Presses, Greenleaf, Bodycote, and Nanocerox. Special thanks to Cliff Bueno and Bill Meade for the use of the data from the 3.5" Inconel phantom. This work was supported by the US DOE, Office of NNSA A&L and MWS Programs, as well as LLNL-LDRD 20-SI-001. It was performed under the auspices of the U.S. Department of Energy by Lawrence Livermore National Laboratory under Contract DE-AC52-07NA27344. LLNL-PRES-824745

REFERENCES

1. J.E. Trebes, et al, Proc. SPIE. 3149, "Developments in X-Ray Tomography," 173, 0277-786X (1997).
2. https://pes-scanning.com/combining-ct-scanning-with-additive-manufacturing/
3. P. Pavan, et al, "Radiation damage and annealing of scintillating glasses," Nucl. Instr. Meth. Phys. Res. B, 61, 487-490 (1991).
4. A. Lempicki, et al, "A new lutetia-based ceramic scintillator for X-ray imaging," Nucl. Instr. Meth. Phys. Res. A, 488, 579 (2002).
5. Z. Seeley, et al, "Two-step sintering of $Gd_{0.3}Lu_{1.6}Eu_{0.1}O_3$ transparent ceramic scintillator," Opt. Mater. Express 3 (7), 908-912 (2013).
6. Z. Seeley, et al, "Phase stabilization in transparent Lu_2O_3: Eu ceramics by lattice expansion," Opt. Mater., 35, 74-78 (2012).
7. N.J. Cherepy, et al, "Transparent ceramic scintillators for gamma spectroscopy and MeV imaging," Proc. SPIE 9593, Hard X-Ray, Gamma-Ray, and Neutron Detector Physics XVII, 95930P (2015).
8. R. Brancaccio, et al., "Real-Time Reconstruction for 3-D CT Applied to Large Objects of Cultural Heritage," IEEE Trans. Nucl. Sci., 58, 4, 1864-1871 (2011).
9. H.E. Martz, C.M. Logan, D.J. Schneberk, P.J. Shull, *X-ray imaging: Fundamentals, industrial techniques, and applications*. (2017).